Variation of Total Electron Content in the Quiet and Disturbed Period and Their Correlation with Solar Wind Parameters

Poonam K.C., Ashok Silwal, Monika Karki, Prakash Poudel, Sujan Prasad Gautam and Devendra Raj Upadhyay

Variation of Total Electron Content in the Quiet and Disturbed Period and Their Correlation with Solar Wind Parameters

Poonam K.C.,[1, a)] Ashok Silwal,[2] Monika Karki,[1] Prakash Poudel,[2] Sujan Prasad Gautam,[3] and Devendra Raj Upadhyay[4, b)]

[1)]*Department of Physics, Amrit Campus, Tribhuvan University, Lainchour - 44600 , Thamel, Kathmandu, Nepal*
[2)]*Department of Physics, Patan Multiple Campus, Tribhuvan University, Patandhoka - 44700 , Lalitpur, Nepal*
[3)]*Central Department of Physics, Tribhuvan University, Kirtipur - 44600 , Kathmandu, Nepal*
[4)]*Amrit Campus, Tribhuvan University, Lainchour - 44600 , Thamel, Kathmandu, Nepal*

[a)]*Corresponding author: punu0504@gmail.com*
[b)]*Electronic mail: devendra.upadhyay@ac.tu.edu.np*

Abstract. Total electron content and electron density are the fundamental parameters that determine the main properties of the ionosphere. We have observed variation of Global Positioning System (GPS) derived Vertical Total Electron Content (VTEC) on three different geomagnetic events. The observed VTEC data is recorded from four GPS stations at different locations ($87.26°$E, $26.48°$N); ($85.79°$E, $27.87°$N); ($84.57°$E, $28.17°$N), and ($86.70°$E, $27.81°$N). To determine the severity of storms, We analysed the north-south component of interplanetary magnetic field (IMF-Bz), solar wind parameters- solar wind speed (Vsw) and solar wind dynamic pressure (Psw) ,and geomagnetic indices- Dst index, Kp index and Auroral Electrojet (AE). For all the studied event days, we observed intensified VTEC on geomagnetically disturbed days over quiet days. The VTEC enhancement was significantly high on the severely disturbed day, followed by the moderate storm and the minor storm.The study made to observe association of VTEC with different interplanetary and geomagnetic indices shows that during all studied event days VTEC enhancement is positively correlated with Vsw, Psw, AE and Kp with cross-correlation coefficient above 0.8 at zero time lag and strong negative correlation with Dst index. In contrast, the correlation of IMF-Bz vary with the intensity of storm. Our finding show a significant variation in VTEC during the geomagnetic disturbances, supporting previous studies on ionospheric responses to geomagnetic storms as well as theoretical assumptions.

INTRODUCTION

The ionosphere is the ionized upper atmosphere of the Earth (located 75 - 1000 km above the Earth). Ionized electrons behave like free particles, delaying signal strength variations, radio propagation, and electromagnetic satellite communications, among other factors [1]. Research on ionospheric behaviour is useful for studying temporal and spatial fluctuations in the ionosphere, as well as forecasting space weather [2]. Space weather is important because of the ionization effect of high-energy solar radiation in the extreme ultraviolet (EUV) and X-ray regions [3, 4]. Satellite systems, energy, transportation, air travel, and hence the economy are all affected by space weather [5].

The corona, the Sun's upper atmosphere, is extremely hot and produces a steady stream of plasma, UV, and X-rays that influence or ionize the ionosphere on Earth. The atoms in this region have been stripped of one or more electrons or ionized as a result of the Sun's tremendous energy and cosmic rays, and are thus positively charged [6]. The nature of the plasma has an impact on electromagnetic signals that interact with it, both natural and man-made. Refraction, absorption, dispersion, and scintillation are all examples of this interaction. Understanding associated communication implications requires the capacity to nowcast and forecast the ionospheric condition and fluctuations on a global scale [7]. Solar forcing, solar EUV flux (photoionization), solar flares, geomagnetic storms [8], and lower atmosphere forcing gravity

waves, thunderstorms, earthquakes, and explosions are all external causes that cause ionosphere variability [9]. The solar wind velocity, temperature, and density change dramatically during a geomagnetic disturbance, along with large variations in the north-south component of the interplanetary magnetic fields (IMF-Bz). However, during quiet periods, measurements on the ground show no significant disturbances [10, 11]. In addition, the geomagnetic storm caused significant ionospheric irregularities in the auroral region [12]. As a result, significant changes in ionospheric parameters such as composition, temperature, and circulation can be observed. Significant disruptions in technical systems, such as static and dynamic location with GNSS satellites, and others, are produced by geomagnetic storms in the Earth's ionosphere [13]. Due to the significant energy introduced by the solar wind into the polar ionosphere (over a period of several hours to a day), there can be an increase or decrease in electron density during geomagnetic storms compared to quiet conditions, which is known as the positive storm effect and negative storm effect, respectively [14]. The storm also had an impact on GPS receiver positioning accuracy: during the storm's main phase, the precise point positioning error exceeded 0.5 m, which is more than five times greater than on quiet day [12].

The vertical total electron content (VTEC) is one of the key quantities used to describe ionosphere variations and can be used by users to correct ionospheric disturbances for GNSS (Global Navigation Satellite System) positioning [15]. Total electron content (TEC) is one of the most significant parameter for investigating the ionosphere, which is linked to many of our planet's unresolved mysteries. The Global Positioning System (GPS) has been an invaluable tool in the research of ionosphere features in recent years [16]. The GPS-TEC is the total number of electrons in a vertical column with a cross section of $1m^2$ from the GPS satellite's height (20, 000 km) to the ground receiver. It's measured in TEC units (TECU), with one TECU equaling 10^{16} electrons m^{-2} [17]. The most significant contributor to GPS position errors is the ionospheric delay, which is proportional to TEC. Thus, TEC is an useful technique for detecting ionospheric changes. Many studies have been conducted on both quiet and disturbed days, and many research have been performed on both [18, 19]. The TEC is affected by the path taken. It can be estimated by integrating the site-dependent electron density ne along the path ds via the ionosphere. Integration along any straight line yields the total slant electron content (STEC).

Using dual frequency GPS data and cases of distinct geomagnetic storms, we investigated the fluctuation of TEC in the ionosphere before and after the geomagnetic storm for four different geographical areas. We selected three solar and geomagnetic storms from 2016, 2017, and 2020. The Kp index and the south-north component of

TABLE I. Stations information.

station	Code	Latitude	Longitude
Biratnagar	BIRT	26.48°N	87.26°E
Sindhuli	SIND	27.87°N	85.79°E
Lamjung	LAMG	28.17°N	84.57°E
Symboche	SYMB	27.81°N	86.70°E

the interplanetary magnetic field, Bz, are used to determine planetary-scale magnetic activity, and they are used to determine events. By measuring the variation of TEC with latitude and longitude for each occurrence, we were able to investigate the storm influence in the ionosphere.

DATABASE AND METHODOLOGY

Data from the Global Positioning System (GPS) ground receivers is used in this study. The data from GPS is stored as RINEX (Receiver Independent Exchange Format) files, which are then converted to ASCII files. We have obtained the data from the UNAVCO data center (`www.unavco.orgdata/gps-gnss/`), which manages GPS/ GNSS data and products from tens of thousands of globally spread permanent stations and campaign sites. GPS data was recorded in universal time (UT = Local Time (LT) + 5:45). As Nodes on the Internet web system, we employed Operating Mission's Internet-based data service (OMNI).

We used data from the OMNI (`http://omniweb.gsfc.nasa.gov/form`) site to observe solar wind particle velocity (Vsw), solar wind pressure (Psw), the southern component of the IMF-Bz, and geomagnetic indices such the Aurora electrojet (AE), the Kp, and Dst indices. The TEC data was transformed to hourly data after 60 seconds. We focused on three events in particular. The first one is a minor storm, the second is indeed a moderate storm and the third is indeed a intense storm. The geomagnetic indices Dst, Kp, and AE were used to evaluate these geomagnetic activities. The Kp and AE indices were used to determine the severity of geomagnetic activities, while the Dst index was used to determine geomagnetic conditions. Minor, moderate, and intense geomagnetic storms are identified by Dst values of ($-50 < Dst < -30$ nT), ($-100 < Dst \leq -50$ nT), and ($-250 < Dst \leq -100$ nT) [3]. We compared TEC to the five quietest days of each month from four GPS stations for each event, and then discussed the cross-correlation of VTEC with other solar wind parameters and geomagnetic indices. The correlation coefficient varies from -1 to +1, with negative and positive values suggesting strong linear fit and values approaching zero indicating poor linear fit. Table I indicates the information related to configuration of GPS stations and Table II indicates the information related to events.

TABLE II. Information of events

Event Date	Geomagnetic Activity	Kp Index
2020/04/20	minor	5-
2016/05/08	moderate	6+
2017/09/08	intense	8+

RESULTS AND DISCUSSION

This section comprises the observation and discussion of geomagnetic indices, solar wind parameters, and VTEC variation on the selected event days. Moreover, we have made a cross-correlation analysis of VTEC with solar wind and geomagnetic parameters which manifests geomagnetic activity.

Observed Geomagnetic Indices and Solar Wind Parameters
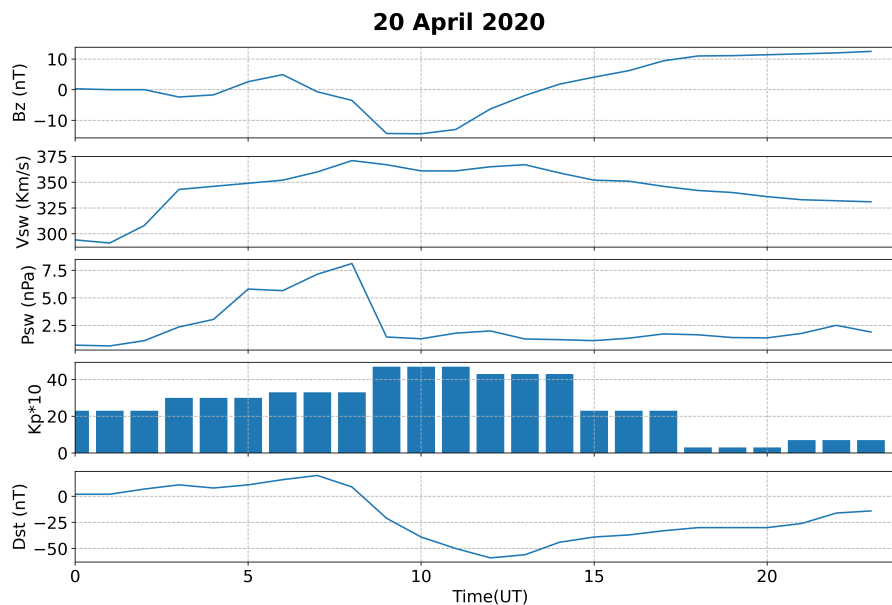
FIGURE 1. From top to bottom, the panels show the variation of the south-north component of Interplanetary magnetic field-Bz (nT) in GSM coordinate system, Flow speed Vsw (km/s), solar wind pressure(nPa), Kp, Dst (nT) with time (UT) respectively.

The study presented in Figure 1 represents variation in interplanetary parameters and geomagnetic indices during a geomagnetic storm that occurred on April 20, 2020. The first row of Figure 1 reveals that by 10 UT, the north-south component of IMF (Bz) value has reduced to a minimum of -11 nT. During this process Magnetic re-connection occurs between the negative IMF and the magnetosphere, opening the field lines with one end connected to the Earth [20]. The phenomena allows protons and electrons to leak in Earth's atmosphere. The flow speed (Vsw) increased from 0 UT to 8 UT as represented in the second row of the Figure. At 8 UT, the streaming reached a peak of 370 km/s. After that, a steady value was reduced, followed by a rise to a second peak value of 365 km/s at 13 UT. The solar wind pressure (Psw) increases from 0 UT reached peak value of 8 nPa at 8UT. Following then, a sharp declination of Psw to 1 nPa is observed. The fourth row reveals that Kp value has not exceeded 5.The Kp-index is the global

geomagnetic activity index that is based on 3-hour measurements from ground-based magnetometers around the world.The fifth row shows Dst index which is the longitudinally averaged part of the external field measured at the geomagnetic dipole equator of the Earth [21]. The minimum value of Dst is recorded -56nT at 12 UT. The observed values of Bz, Dst, Kp and flow speed (Vsw) indicate that the geomagnetic event of April 20, 2020 is a minor geomagnetic storm. The minor events occur at a rate of 1700 per cycle (1 cycle = 11 years), posing a slight threat to satellite.

Figure 2 presents the variation in studied solar wind and geomagnetic parameters during storm event of 08 May 2016. Figure shows that field strength Dst decreases dramatically during the storm main phase which typically lasts for about 8 hours (1 UT to 8 UT). During this period Dst value is declined from 1 nT to -72 nT indicating the moderate geomagnetic storm [3]. Moderate events oc-

08 May 2016
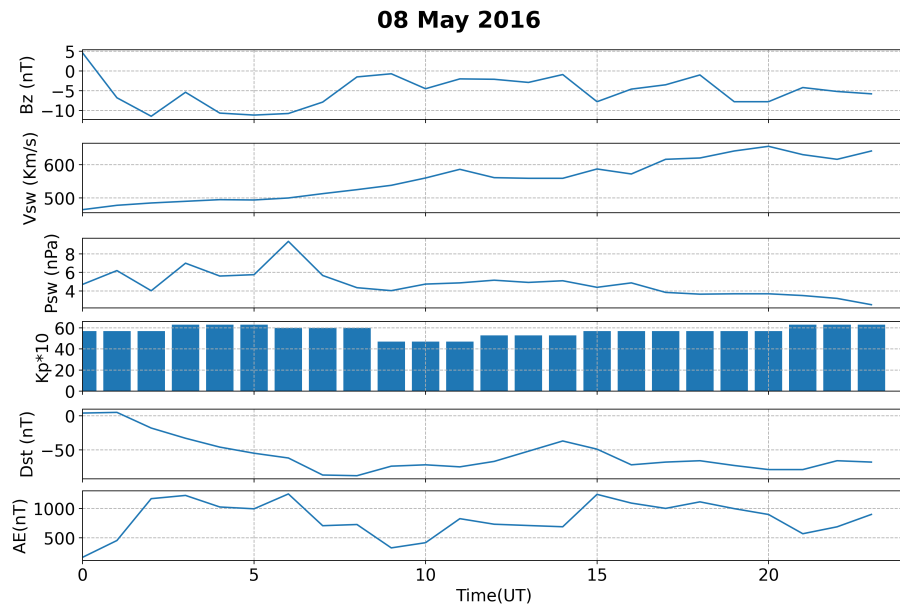
FIGURE 2. From top to bottom, the panels show the variation of the south-north component of Interplanetary magnetic field-Bz (nT) in GSM coordinate system, Flow speed Vsw (km/s), solar wind pressure(nPa), Kp, Dst (nT)and AE (nT) indices with time (UT) respectively.

08 September 2017
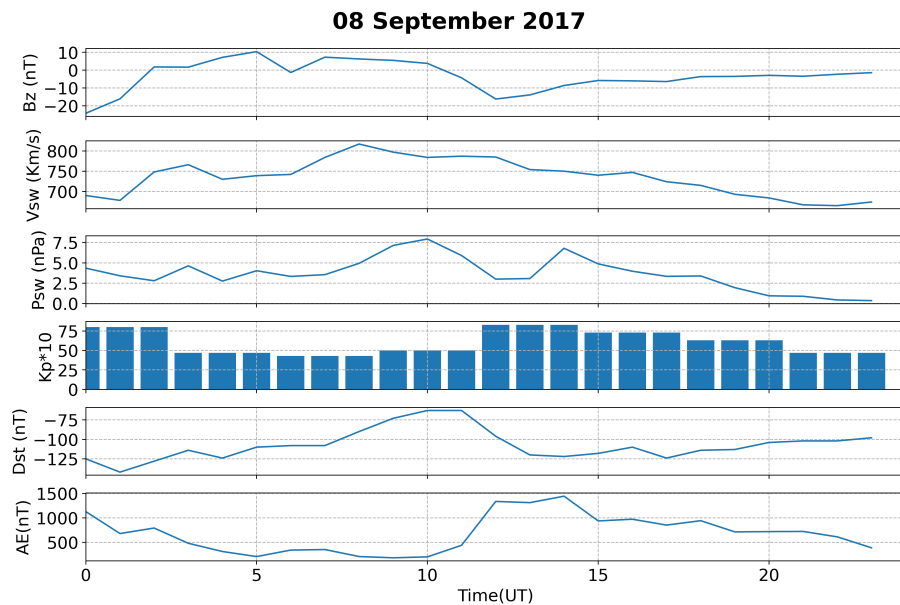
FIGURE 3. From top to bottom, the panels show the variation of the south-north component of Interplanetary magnetic field-Bz (nT) in GSM coordinate system, Flow speed Vsw (km/s), solar wind pressure (nPa), Kp, Dst (nT) and AE (nT) indices with time (UT) respectively.

cur at an average of 600 times per 11 years, which might cause HF radio transmission to decline at higher latitudes. The main phase of storm is due to increase in the ring current, resulting from an enhanced particle flow towards the Earth [22]. This event is remarked with large variability in near Earth solar wind condition. As witnessed from first row of the Figure 2 the IMF Bz turned towards south direction from first hour of the day reaching minimum of -11 nT, at 5 UT. It is well known that geomagnetic storms tend to occur when IMF is directed southward.

A larger southward Bz value allows for a more effective energy transfer from the Sun's magnetic field lines to the Earth's magnetosphere [20]. The second row of the Figure shows the increment of solar wind velocity from 0 UT to 11 UT streaming a maximum of 590 km/s. Following that, a stable value was maintained before increasing to its second peak of 625 km/s at 20 UT. The solar wind pressure (Psw) increases from 0 UT to 6 UT attaining the peak value of 9 nPa. During the geomagnetic storm, the enhancement in the pressure and speed of solar wind is due to the strong shock found ahead of fast coronal mass ejections [23]. The Kp value is recorded within 4 and 6 throughout the day. Similarly, the AE index varies from 0 to a peak of 1290 nT. While the AE index value is tens of nT during a quiet period, it jumps to several hundred and more than a thousand nT during storms and sub-storms [24]. The variation in interplanetary and geomagnetic conditions during storm event of 08 September 2017 is represented in Figure 3. This space weather event is probably the most studied event of solar cycle 24 [25, 26, 27, 28] as the storm was characterized by two pronounced Dst minima within time interval of few hours on the same day. As witnessed from Figure 3, the first minimum is observed at 2UT (-142 nT), and second at 14 UT (-122 nT). Both minimum were accompanied by shock wave of the Coronal Mass Ejection (CME) from the solar surface [29]. The detail of this event can be fond in dimmock et al., (2019) [30]. The first row of Figure 3 shows that the Bz with value -24.2nT at the starting of the day, in southward direction steadily turned to north gaining the amplitude of 10.4 nT at about 5 UT. After 10 UT, Bz is again turned toward south maintainig the peak value of -18nT at around 13 UT. This southward leading magnetic field are associated with stronger geomagnetic storms [31]. The second row of the Figure illustrates the inclining speed of plasma until a large forward shock arrives near 08:00 UT. The significant increase in speed from approximately 600 km/h to more than 830 km/h is a indication of the shock. The solar wind pressure (Psw) also increased until 10 UT to reach a peak of 7.5 nPa. This enhancement in solar wind dynamic pressure during southward IMF configuration is attributed to solar wind-magnetosphere coupling and increment in ring current injection rate [32, 33]. Kp index is recorded 8 during the peak phase of storm event. Kp is the largest difference between the highest and the lowest values of X and Y components of geomagnetic field [34, 35]. Similarly, the AE index in the last row swings from 0 to a peak of 1442 nT about 14 UT. AE-index serves to estimate the global electrojet activity in the auroral zone [36]. The recorded value of solar wind parameters and geomagnetic indices shows that the event of 8 Sepetember, 2017 is intense geomagnetic storm. These type of geomagnetic storms causes surface charging and tracking issues for satellite system.

VTEC Variation during Geomagnetic Activity

Fig. 4 compares the variation of TEC during a minor storm event of April 20, 2020 with mean TEC of the most five quietest days of same month of 2020 at BIRT, SIND, LAMG, and SYMB GPS stations. In general, the diurnal variation of TEC is lowest in the pre-dawn, has a constant incline in the early morning, a maximum TEC value in the afternoon, and then progressively decreases after sunset. This pattern of diurnal variation of VTEC is very expected phenomena because ionization process in upper atmosphere increases with increment in solar radiation intensity. From all locations, the value of TEC was greater on disturbed days than on quiet days, as shown in Figure 4. The peak value of VTEC in both quiet and disturbed day is found to be around 8 UT. The day time peak TEC values depend greatly on the strength of the equatorial ionization anomaly in the low latitude regions [37]. The difference in VTEC between disturbed day and the quiet days is found to vary between 3-7 TECU.The change in VTEC in storm time can be attributed to prompt penetration of electric field originated due to the under-shielding and over-shielding conditions, and traveling atmospheric disturbances [38, 39].
Fig. 5 compares the TEC variability during a storm event of May 8, 2016 with mean TEC of the most five quietest days of May, 2016 over the studied GPS stations. One can observe that both disturbed day and quiet day followed the diurnal pattern of VTEC in case of a moderate storm event. It is observed that VTEC value of storm day overestimate quiet day VTEC from 2 UT to 22 UT. The peak value reached above 50 TECU at 8 UT during the event day. At the same time of the day, VTEC peak with value around 40 TECU is discovered in quiet days. As there is an increase in the ionospheric electron content in event day in relation to quiet days, the geomagnetic storm of may 8, 2016 is positive ionospheric storm. The mechanisms that enhance the occurrence of positive ionospheric response can be found in Goncharenko et al.,(2007) [40] and Huang et al.,(2005) [41]. Moderate geomagnetic storms strongly disturb the equatorial and low-latitude space-time evolution of VTEC and the ionospheric electrodynamics compared with quiet days [42].

Fig. 6 shows the variation of the TEC during the intense geomagnetic storm of 8 September 2017, along with the mean TEC of the top five quietest days of the same month of 2017. This Figure reveals a considerable in-
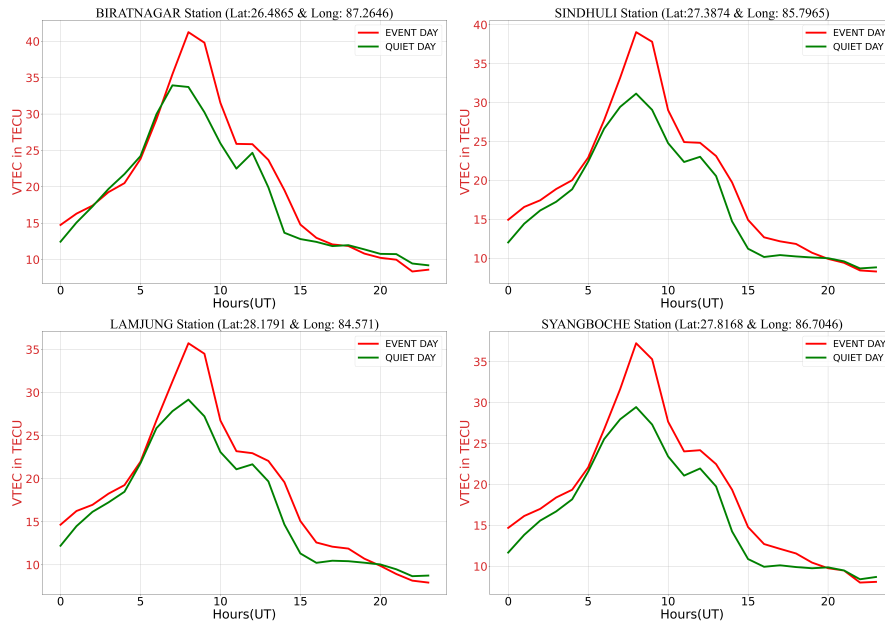
FIGURE 4. Comparison of TEC variability during a minor storm event of April 20, 2020 with mean TEC of the most five quietest days of the same month at BIRT, SIND, LAMG, and SYMB GPS stations resectively.
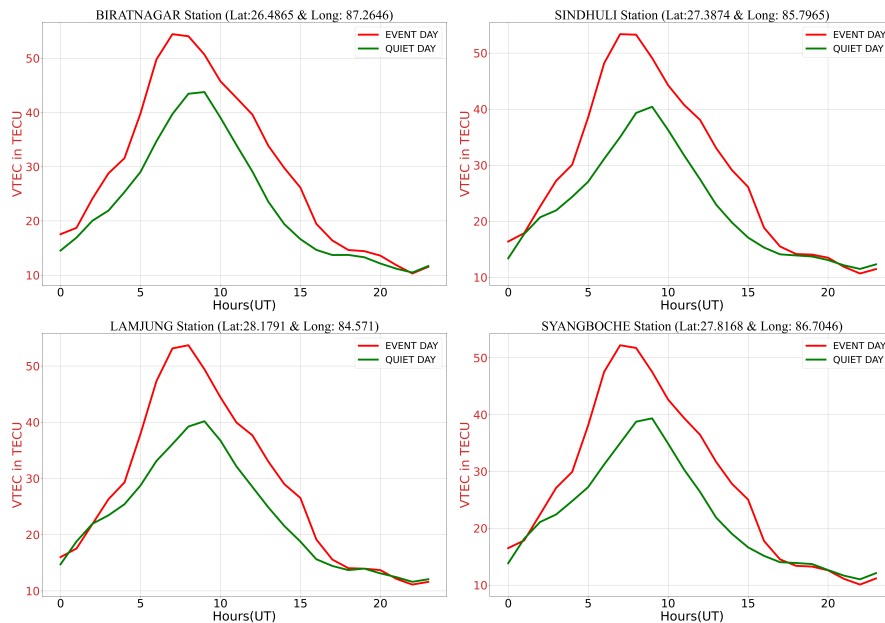
FIGURE 5. Comparison of TEC variability during a moderate storm event of May 8, 2016 with mean TEC of the most five quietest days of the same month at BIRT, SIND, LAMG, and SYMB GPS stations resectively.

crease in the VTEC value during the storm when comparing a storm day to a quiet day. During this geomagnetic event, the diurnal variation pattern of the minimum VTEC in the predawn hours was not followed as in previ-
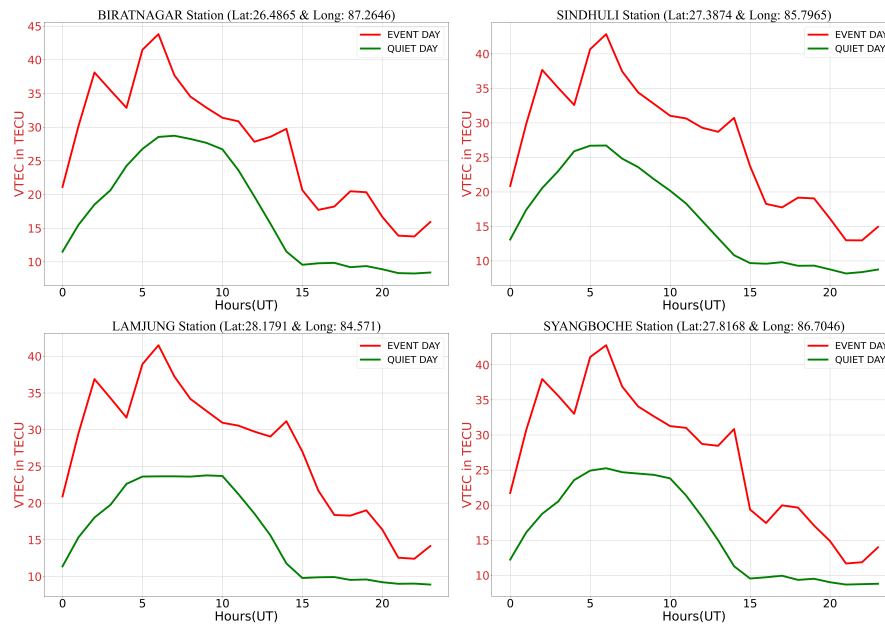
FIGURE 6. Comparison of TEC variability during a intense storm event of September 8,2017 with mean TEC of the most five quietest days of of the same month at BIRT, SIND, LAMG, and SYMB GPS stations resectively.

ous studied events. This could be due to the fact that the day's initial few hours were spent in the midst of a intense geomagnetic storm (refer previous section) developed at late night hour of previous day [28]. It is interesting to note multistep VTEC variation on this geomagnetic event i.e., it first sharply increased during 0-3 UT, then it suddenly decreased at 04 UT and again started increasing to attain a peak value of 44 TECU, 43 TECU, 42 TECU and 43 TECU at BIRT, SIND, LAMG, and SYMB stations,

respectively, exactly at the same time, 06:00 UT. Then, it gradually decreased for the remaining time period. In addition, we noticed a slight increase in the VTEC value around 14:00 UT. It could be related to the second phase of the storm that occurred at 14:00 UT. This VTEC enhancements can be attributed to the combined impacts of Prompt Penetration Electric Fields (PPEFs) and suddenly increased extreme ultraviolet (EUV) radiations and X-rays accompanied with the solar flare [27, 43].

Cross-Correlation Analysis

Cross-correlation is the measurement to establish the relationship between two time series data. Several early researchers considered it as a robust tool to compare multiple time series and employed it to study Relativistic electron flux [44], solar eclipse [45, 46, 47], solar wind parameters [48], and now also for seismic activities [49]. Fig. 7a, 7b, and 7c demonstrate the plot of cross-correlation of mean hourly VTEC data of LAMG GPS station with mean hourly VTEC data of BIRT, SIND, and SYMB GPS stations during minor, moderate and intense geomagnetic storms. The horizontal axis depicts the time

During the minor geomagnetic storm that occurred on April 20, 2020, the cross-correlation results of VTEC with IMF-Bz, Vsw, Psw, Kp, and Dst are shown in Figure 8a. The yellow curve (VTEC-Kp), blue curve (VTEC-

scale in hours, which goes from (-24 to 24), while the vertical axis depicts the cross-correlation coefficient, which ranges from (-1 to +1). Following the correlation of the indices, time scales are utilized to identify the lead or lag between them. The Figures showed a substantial positive correlation between mean hourly VTEC data from the LAMG GPS station and data from other stations with a cross-correlation coefficient of +1 at zero time lag. This result simplifies the selection of the LAMG GPS station as a reference station, and it has been used to represent all other stations in this study.

Vsw), and red curve (VTEC-Psw) in the Figure demonstrate a negative correlation coefficient ranging from -0.19 at a time lag of -4 hours to 0.61 at +12 hours. The black curve (VTEC-Dst) illustrates the nature of mod-
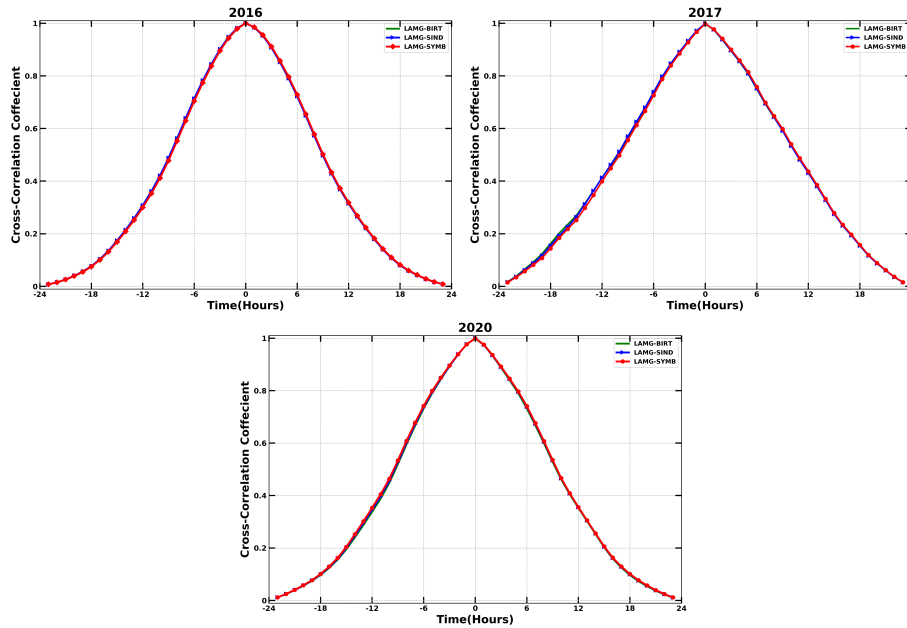
FIGURE 7. Cross-correlation of mean hourly VTEC data obtained from LAMG GPS station with VTEC data from BIRT, SIND and SYMB GPS stations on a) 08 MAY 2016 b) 08 SEPTEMBER 2017 and c) 20 APRIL 2020.
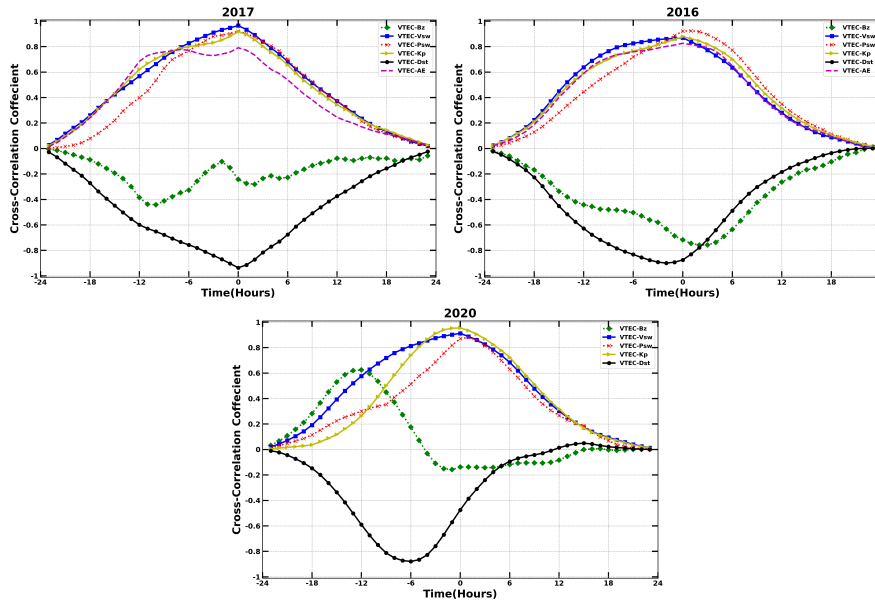
FIGURE 8. Cross-correlation of GPS VTEC with the component of Interplanetary magnetic field IMF-Bz (nT) in GSM coordinate system, Flow speed Vsw (km/s), Flow pressure Psw , Kp (nT), Dst (nT) and AE (nT) on a) 08 SEPTEMBER 2017 b) 08 MAY 2016 and c) 20 APRIL 2020.

erate correlation, which crosses the zero point with a cross-correlation coefficient that spans from +0.12 at 12 hour time lags to -0.87 at -6 hour time lags. VTEC-IMF-Bz (green curve) has a similar nature, with a coefficient ranging from -0.19 at a time lag of -4 hours to 0.615 at +12 hours. Similarly, with zero-time lag, the yellow

(VTEC-Kp) and blue (VTEC-Vsw) curves indicate a high positive correlation with amplitudes of 0.94 and 0.90, respectively. The plots of the red curve (VTEC-Psw) also reveal a positive association with a maximum amplitude of 0.8634 at a 2 hour time lag. The plots of the black (VTEC-Dst) and green (VTEC-IMF-BZ) curves are a lit-

tle unsymmetrical when compared to cross-correlation plots of the other events.

During a moderate geomagnetic storm on May 8, 2016, the cross-correlation results of VTEC with IMF-Bz, Vsw, Psw, Kp, Dst, and AE are shown in Fig. 8b. When they are in the same phase, i.e. lag zero, the red (VTEC-Psw), blue (VTEC-Vsw), and yellow curves demonstrate a good positive correlation of VTEC with Psw, Vsw, and Kp with maximum cross-correlation coefficient values of 0.94, 0.86, and 0.82, respectively. At a zero-time lag, the magenta curve (VTEC-AE) similarly exhibits a positive connection, with a correlation coefficient of 0.81. At zero-time lag, the green (VTEC-Bz) and black (VTEC-Dst) curves preserved amplitudes of -0.66 and -0.84, respectively, indicating a negative correlation between VTEC and IMF-Bz and Dst.

During the intense geomagnetic storm day on September 8, 2017, the cross-correlation results of VTEC with IMF-Bz, Vsw, Psw, Kp, Dst, and AE are shown in Fig. 8. The mean hourly VTEC value of the LAMG GPS station was utilized since, as previously stated, it demonstrated a significant correlation with data from other stations. The yellow (VTEC-Kp), blue (VTEC-Vsw), and red (VTEC-Psw) curves practically overlap throughout the lag -24 to +24 hours in the Figure, with a maximum correlation coefficient of 0.93 at zero-time lag, indicating the significant positive correlation of VTEC with Kp, Vsw, and Psw when they are in phase. At a zero-time lag, the magenta curve (VTEC-AE) similarly exhibits a positive association with a correlation coefficient of 0.79. At zero-time lag, the green (VTEC-Bz) and black (VTEC-Dst) curves maintained amplitudes of -0.415 and -0.946, respectively, indicating a negative correlation of VTEC with IMF-Bz and Dst. Furthermore, the greatest value achieved by the green curve and black curve at +2 hours and -10 hours time lags, respectively, demonstrates that VTEC had led IMF-Bz and Dst by 2 hours and 10 hours before they correlated.

CONCLUSION

We presented a study on the behaviour of GPS derived VTEC on three different geomagnetically disturbed days. The event days were categorized from minor to intense by analyzing the geomagnetic indices- Kp index, Dst values, and AE index, as well as solar wind parameters- solar wind speed, interplanetary magnetic field, and solar wind pressure . The study was made using TEC derived by dual frequency GPS receivers deployed at four different locations: (87.26°E, 26.48°N); (85.79°E, 27.87°N); (84.57°E, 28.17°N); and (86.70°E, 27.81°N). Our results can be summerized as follow:

The diurnal variation pattern of VTEC was preserved in a minor and moderate storm day, i.e., minimum in the predawn, maximum during day hours, and then again drops during the night. A similar pattern with low amplitute VTEC peak was followed in quiet days. However, during the case of a severe geomagnetic storm, we noticed an unusual diurnal pattern with several VTEC peaks throughout the day, which might have occurred due to the development of the geomagnetic storm in the late nights hours of the day before the main event and another shock wave experienced at the mid-day time of event day.

The VTEC enhancement was significantly high on the severely disturbed day, followed by the moderate storm and the minor storm. Overall, the positive ionospheric storm effects are observed in all event days. Imtiaz et al 2020 have associated positive ionospheric response with the ionospheric electric fields and the traveling atmospheric disturbances. The variety of space weather phenomena such as the solar flare, coronal mass ejection, the high speed solar wind stream contributes to the enhanced TEC [50].

Cross-correlation analysis presented the association of VTEC value with solar wind parameters and geomagnetic indices. The VTEC value shows a strong positive association with solar wind velocity, Kp index and solar wind dynamic pressure and AE. The Dst-index is negatively associated with VTEC during minor and moderate storm days with relatively less time lag; however, at 0 hrs time lag during intense storm. The north-south component of IMF shows good negative correlation with VTEC in severe storm day and feeble negative correlation in moderate storm event but we observed positive as well as negative association of VTEC and Bz at different time lags in minor event day. Thus, it is suggested not to rely solely on one interplanetary or geomagnetic parameter in a study of specific events especially if one desire to monitor Ionospheric characterstics during geomagnetic storms.

Studying the Ionosphere of Nepal during geomagnetic storms we found that the GPS measurement of ionospheric TEC is quite effective in monitoring space weather activities. These type of studies are crucial to monitor the solar activities and ionospheric response during multiple space weather events so that we can mitigate possible hazards in our infrastructures like radio signal disruption, power grid fluctuations, voltage control problems, induced pipeline currents, and satellite orientation. We believe that this study would serve as a baseline for providing crucial information on ionospheric variability over Himalayan territory region, and future researchers can use these data to improve models of ionospheric dynamics. Further investigation with the use of different statistical and computational tool is suggested to explore this observation.

ACKNOWLEDGMENTS

REFERENCES

1. A. Krypiak-Gregorczyk, "Ionosphere response to three extreme events occurring near spring equinox in 2012, 2013 and 2015, observed by regional gnss-tec model," Journal of Geodesy **93**, 931–951 (2019).

2. W. Zhang, X. Zhao, S. Jin, and J. Li, "Ionospheric disturbances following the march 2015 geomagnetic storm from gps observations in china," Geodesy and Geodynamics **9**, 288–295 (2018).

3. W. Gonzalez, J.-A. Joselyn, Y. Kamide, H. W. Kroehl, G. Rostoker, B. Tsurutani, and V. Vasyliunas, "What is a geomagnetic storm?" Journal of Geophysical Research: Space Physics **99**, 5771–5792 (1994).

4. N. P. Chapagain, *Dynamics of equatorial spread F using ground-based optical and radar measurements* (Utah State University, 2011).

5. C. J. Schrijver, K. Kauristie, A. D. Aylward, C. M. Denardini, S. E. Gibson, A. Glover, N. Gopalswamy, M. Grande, M. Hapgood, D. Heynderickx, *et al.*, "Understanding space weather to shield society: A global road map for 2015-2025 commissioned by cospar and ilws," Advances in Space Research **55**, 2745–2807 (2015).

6. B. Adhikari, B. Kaphle, N. Adhikari, S. Limbu, A. Sunar, R. K. Mishra, and S. Adhikari, "Analysis of cosmic ray, solar wind energies, components of earth's magnetic field, and ionospheric total electron content during solar superstorm of november 18-22, 2003," SN Applied Sciences **1**, 1–10 (2019).

7. E. H. Lay, J. D. Tippmann, K. C. Wiens, S. E. McDonald, A. J. Mannucci, X. Pi, A. Coster, R. M. Kippen, M. J. Peterson, and R. Redmon, "New lightning-derived vertical total electron content data provides unique global ionospheric measurements," Space Weather , e2022SW003067 (2022).

8. W. Wang, J. Lei, A. G. Burns, S. C. Solomon, M. Wiltberger, J. Xu, Y. Zhang, L. Paxton, and A. Coster, "Ionospheric response to the initial phase of geomagnetic storms: Common features," Journal of Geophysical Research: Space Physics **115** (2010).

9. E. H. Lay, "Ionospheric irregularities and acoustic/gravity wave activity above low-latitude thunderstorms," Geophysical Research Letters **45**, 90–97 (2018).

10. S. Sharma, P. Galav, N. Dashora, S. Alex, R. Dabas, and R. Pandey, "Response of low-latitude ionospheric total electron content to the geomagnetic storm of 24 august 2005," Journal of Geophysical Research: Space Physics **116** (2011).

11. N. Bhattarai, N. P. Chapagain, and B. Adhikari, "Study of total electron content-tec and electron density profile during geomagnetic storms," arXiv preprint arXiv:1803.06066 (2018).

12. E. Astafyeva, Y. V. Yasyukevich, B. Maletckii, A. Oinats, A. Vesnin, A. Yasyukevich, S. Syrovatskii, and N. Guendouz, "Ionospheric disturbances and irregularities during the 25-26 august 2018 geomagnetic storm," Journal of Geophysical Research: Space Physics **127**, e2021JA029843 (2022).

13. M. J. Buonsanto, "Ionospheric storms—a review," Space Science Reviews **88**, 563–601 (1999).

14. T. Fuller-Rowell, M. Codrescu, R. Moffett, and S. Quegan, "Response of the thermosphere and ionosphere to geomagnetic storms," Journal of Geophysical Research: Space Physics **99**, 3893–3914 (1994).

15. G. O. Jerez, M. Hernández-Pajares, A. Goss, C. M. da Silva, D. Alves, and J. F. Monico, "Impact and synergies of gim error estimates on the vtec interpolation and single-frequency ppp at low latitude region," GPS Solutions **26**, 1–13 (2022).

16. S. Karia and K. Pathak, "Gps based tec measurements for a period august 2008-december 2009 near the northern crest of indian equatorial ionospheric anomaly region," Journal of Earth System Science **120**, 851–858 (2011).

17. V. Chauhan, O. Singh, and B. Singh, "Diurnal and seasonal variation of gps-tec during a low solar activity period as observed at a low latitude station agra," 94.20. dv; 96.60. qd (2011).

18. P. Xiong, D. Zhai, C. Long, H. Zhou, X. Zhang, and X. Shen, "Long short-term memory neural network for ionospheric total electron content forecasting over china," Space Weather **19**, e2020SW002706 (2021).

19. C. Cesaroni, L. Spogli, A. Aragon-Angel, M. Fiocca, V. Dear, G. De Franceschi, and V. Romano, "Neural network based model for global total electron content forecasting," Journal of Space Weather and Space Climate **10**, 11 (2020).

20. J. Dungey, "The structure of the exosphere, or adventures in velocity space," Geophysics, the Earth's environment (1963).

21. M. Sugiura and C. R. Wilson, "Oscillation of the geomagnetic field lines and associated magnetic perturbations at conjugate points," Journal of Geophysical Research **69**, 1211–1216 (1964).

22. S. Yousef, M. El Nawawy, M. El-Nazer, and M. Yousef, "Successive impacts of the earth by several halo cmes from active region noaa 652," Proceedings of the International Astronomical Union **2004**, 477–478 (2004).

23. R. T. Desai, M. P. Freeman, J. P. Eastwood, J. W. Eggington, M. O. Archer, Y. Shprits, N. P. Meredith, F. A. Staples, I. J. Rae, H. Hietala, *et al.*, "Interplanetary shock-induced magnetopause motion: Comparison between theory and global magnetohydrodynamic simulations," Geophysical Research Letters **48**, e2021GL092554 (2021).

24. G. Rostoker, "Geomagnetic indices," Reviews of Geophysics **10**, 935–950 (1972).

25. Y. Yasyukevich, E. Astafyeva, A. Padokhin, V. Ivanova, S. Syrovatskii, and A. Podlesnyi, "The 6 september 2017 x-class solar flares and their impacts on the ionosphere, gnss, and hf radio wave propagation," Space Weather **16**, 1013–1027 (2018).

26. J. Lei, F. Huang, X. Chen, J. Zhong, D. Ren, W. Wang, X. Yue, X. Luan, M. Jia, X. Dou, *et al.*, "Was magnetic storm the only driver of the long-duration enhancements of daytime total electron content in the asian-australian sector between 7 and 12 september 2017?" Journal of Geophysical Research: Space Physics **123**, 3217–3232 (2018).

27. S. Kumar and S. Kumar, "Equatorial ionospheric tec and scintillations under the space weather events of 4-9 september 2017: M-class solar flares and a g4 geomagnetic storm," Journal of Atmospheric and Solar-Terrestrial Physics **209**, 105421 (2020).

28. Y. Liu, Z. Li, L. Fu, J. Wang, and C. Zhang, "Studying the ionospheric responses induced by a geomagnetic storm in september 2017 with multiple observations in america," GPS Solutions **24**, 1–13 (2020).

29. D. Blagoveshchensky and M. Sergeeva, "Impact of geomagnetic storm of september 7-8, 2017 on ionosphere and hf propagation: A multi-instrument study," Advances in Space Research **63**, 239–256 (2019).

30. A. P. Dimmock, L. Rosenqvist, J.-O. Hall, A. Viljanen, E. Yordanova, I. Honkonen, M. André, and E. Sjöberg, "The gic and geomagnetic response over fennoscandia to the 7-8 september 2017

geomagnetic storm," Space Weather **17**, 989–1010 (2019).

31. A. A. Pevtsov and R. C. Canfield, "Solar magnetic fields and geomagnetic events," Journal of Geophysical Research: Space Physics **106**, 25191–25197 (2001).

32. C. Wang, J. Chao, and C.-H. Lin, "Influence of the solar wind dynamic pressure on the decay and injection of the ring current," Journal of Geophysical Research: Space Physics **108** (2003).

33. B. Adebesin, S. Ikubanni, J. Kayode, and B. Adekoya, "Variability of solar wind dynamic pressure with solar wind parameters during intense and severe storms," The African Review of Physics **8** (2013).

34. J. Bartels, "The standardized index ks, and the planetary index kp, iatme bull., 12 (b), 97, iugg publ," Office, Paris (1949).

35. J. Matzka, C. Stolle, Y. Yamazaki, O. Bronkalla, and A. Morschhauser, "The geomagnetic kp index and derived indices of geomagnetic activity," Space Weather **19**, e2020SW002641 (2021).

36. T. N. Davis and M. Sugiura, "Auroral electrojet activity index ae and its universal time variations," Journal of Geophysical Research **71**, 785–801 (1966).

37. M. S. Bagiya, H. Joshi, K. Iyer, M. Aggarwal, S. Ravindran, and B. Pathan, "Tec variations during low solar activity period (2005-2007) near the equatorial ionospheric anomaly crest region in india," in *Annales Geophysicae*, Vol. 27 (Copernicus GmbH, 2009) pp. 1047–1057.

38. N. Dashora, S. Sharma, R. Dabas, S. Alex, and R. Pandey, "Large enhancements in low latitude total electron content during 15 may 2005 geomagnetic storm in indian zone," in *Annales Geophysicae*, Vol. 27 (Copernicus GmbH, 2009) pp. 1803–1820.

39. R. Trivedi, A. Jain, S. Jain, and A. Gwal, "Study of tec changes during geomagnetic storms occurred near the crest of the equatorial ionospheric ionization anomaly in the indian sector," Advances in space research **48**, 1617–1630 (2011).

40. L. Goncharenko, J. Foster, A. Coster, C. Huang, N. Aponte, and L. Paxton, "Observations of a positive storm phase on september 10, 2005," Journal of atmospheric and solar-terrestrial physics **69**, 1253–1272 (2007).

41. C.-S. Huang, J. Foster, L. Goncharenko, P. Erickson, W. Rideout, and A. Coster, "A strong positive phase of ionospheric storms observed by the millstone hill incoherent scatter radar and global gps network," Journal of Geophysical Research: Space Physics **110** (2005).

42. B. Ribeiro, P. Fagundes, K. Venkatesh, A. Tardelli, V. Pillat, and G. Seemala, "Equatorial and low-latitude positive ionospheric phases due to moderate geomagnetic storm during high solar activity in january 2013," Advances in Space Research **64**, 995–1010 (2019).

43. A. Singh, V. S. Rathore, S. Kumar, S. Rao, S. K. Singh, and A. Singh, "Effect of intense geomagnetic storms on low-latitude tec during the ascending phase of the solar cycle 24," Journal of Astrophysics and Astronomy **42**, 1–11 (2021).

44. P. Poudel, N. Parajuli, A. Gautam, D. Sapkota, H. Adhikari, B. Adhikari, A. Silwal, S. Gautam, M. Karki, and R. Mishra, "Wavelet and cross-correlation analysis of relativistic electron flux with sunspot number, solar flux, and solar wind parameters," Journal of Nepal Physical Society **6**, 104–112 (2020).

45. A. Silwal, S. Gautam, N. Chapagain, M. Karki, P. Poudel, B. Ghimire, R. Mishra, and B. Adhikari, "Ionospheric response over nepal during the 26 december 2019 solar eclipse," Journal of Nepal Physical Society **7**, 25–30 (2021).

46. A. Silwal, S. Gautam, P. Poudel, M. Karki, B. Adhikari, N. Chapagain, R. Mishra, B. Ghimire, and Y. Migoya-Orue, "Global positioning system observations of ionospheric total electron content variations during the 15th january 2010 and 21st june 2020 solar eclipse," Radio Science **56**, 1–20 (2021).

47. B. D. Ghimire, A. Silwal, N. P. Chapagain, S. P. Gautam, P. Poudel, and B. Khadka, "Gps observations of ionospheric tec variations over nepal during 22 july 2009 solar eclipse," EUREKA: Physics and Engineering,(2) , 3–14 (2022).

48. A. Silwal, S. P. Gautam, K. Chaudhary, M. Khanal, S. Joshi, S. Dangaura, and B. Adhikari, "Study of solar wind parameters during geomagnetic storm of 26th august 2018 and 28th september 2017," Thai Journal of Physics **38**, 54–68 (2021).

49. M. Karki, A. Silwal, N. P. Chapagain, P. Poudel, S. P. Gautam, R. K. Mishra, B. Adhikari, and Y. O. M. Orue, "Gps observations of ionospheric tec variations during 2015 mw 7.8 nepal earthquake," Earth and Space Science Open Archive ESSOAr (2020).

50. P. O. Amaechi, A. O. Akala, J. O. Oyedokun, K. Simi, O. Aghogho, and E. O. Oyeyemi, "Multi instrument investigation of the impact of the space weather events of 6-10 september 2017," Space Weather , e2021SW002806 (2021).